

1/f Noise in epitaxial sidewall graphene nanoribbons

Cite as: Appl. Phys. Lett. **117**, 083105 (2020); <https://doi.org/10.1063/5.0020926>

Submitted: 06 July 2020 . Accepted: 19 August 2020 . Published Online: 26 August 2020

O. Vail, J. Hankinson, C. Berger, W. A. de Heer, and Z. Jiang 



View Online



Export Citation



CrossMark

ARTICLES YOU MAY BE INTERESTED IN

[Electrically tunable high Curie temperature two-dimensional ferromagnetism in van der Waals layered crystals](#)

Applied Physics Letters **117**, 083102 (2020); <https://doi.org/10.1063/5.0014865>

[Empowering 2D nanoelectronics via ferroelectricity](#)

Applied Physics Letters **117**, 080503 (2020); <https://doi.org/10.1063/5.0019555>

[Structural disorder, sublattice melting, and thermo-elastic properties of anti-perovskite Li₃OBr under high pressure and temperature](#)

Applied Physics Letters **117**, 081904 (2020); <https://doi.org/10.1063/5.0018714>

Lock-in Amplifiers
up to 600 MHz



Watch



1/f Noise in epitaxial sidewall graphene nanoribbons

Cite as: Appl. Phys. Lett. **117**, 083105 (2020); doi: [10.1063/5.0020926](https://doi.org/10.1063/5.0020926)

Submitted: 6 July 2020 · Accepted: 19 August 2020 ·

Published Online: 26 August 2020



View Online



Export Citation



CrossMark

O. Vail,¹ J. Hankinson,¹ C. Berger,^{1,2} W. A. de Heer,^{1,3} and Z. Jiang^{1,a)} 

AFFILIATIONS

¹School of Physics, Georgia Institute of Technology, Atlanta, Georgia 30332, USA

²UMI 2958 Georgia Tech-CNRS 2, rue Marconi, 57070 Metz, France

³Tianjin International Center of Nanoparticles and Nanosystems, Tianjin University, 300072 Tianjin, China

^{a)}Author to whom correspondence should be addressed: zhigang.jiang@physics.gatech.edu

ABSTRACT

We perform gate- and temperature-dependent low-frequency noise measurements on epitaxial graphene nanoribbons (epiGNRs) grown on the sidewalls of trenches etched in SiC substrates. We find that the measured noise spectra are dominated by 1/f noise, and the main source of the noise at high carrier densities is the long-range scatters (charge traps) at the epiGNR/gate-dielectric interface. Interestingly, our findings differentiate sidewall epiGNRs from previously studied lithographically patterned GNRs while exhibiting competitive noise characteristics similar to those in high-quality suspended graphene or graphene on hexagonal boron nitride substrates. These results provide confidence in potential epiGNR-based device applications in low-noise nanoelectronics.

Published under license by AIP Publishing. <https://doi.org/10.1063/5.0020926>

Graphene is an atomically thin structure composed of sp^2 -bonded carbon atoms arranged in a hexagonal lattice. In addition to its sub-nanoscale dimension, graphene has been shown to exhibit many intriguing transport phenomena, including high mobility, tunable carrier concentration, and ballistic transport at room temperature.^{1–4} For these and other beneficial electronic, chemical, and mechanical properties, the scientific and technological community has been rapidly gaining interest in nanostructuring graphene to form different prototype devices. Among various graphene nanostructures, graphene nanoribbons (GNRs) stand out owing to their promise as a one-dimensional ballistic conductor or channel material for field-effect-transistors (FETs),^{4–8} following more than two decades intensive research on carbon nanotubes (CNTs). However, controlling the electronic properties of CNTs proves difficult,⁹ and chemically or lithographically fabricated GNRs suffer from edge disorder and the resulting electron localization.^{7,8,10} A new route is needed for nanopatterning graphene without sacrificing its intrinsic properties.

Epitaxial graphene grown on electronics-grade SiC is an ideal platform for developing graphene nanoelectronics.^{11,12} In particular, epitaxial growth on the sidewall of a SiC nanostep enables the production of long, narrow GNRs with preserved crystalline edges, exhibiting exceptional mean free paths of $\sim 10 \mu\text{m}$ at room temperature.^{4,13,14} With these superb properties, epitaxial GNRs (epiGNRs) provide promising possibilities for advanced device applications.

A determinative factor for the performance of graphene FETs and sensors is the inherent noise level that limits input sensitivity.¹⁵ In this Letter, we report on a systematic study of the low-frequency electrical noise in sidewall epiGNRs with respect to gate voltage and temperature. We show that the measured noise spectra are 1/f-like, and the dominant noise source at high carrier densities is long-range scatters, presumably at the epiGNR/gate-dielectric interface. We also compare the noise amplitude of sidewall epiGNR with other carbon systems and demonstrate its potential in future graphene-based nanoelectronics.

The epiGNRs studied in this work were selectively grown along the zigzag direction on the sidewalls of insulating 4H-SiC substrates by the confinement controlled sublimation method.^{13,16} Before the growth, the SiC(0001) face was pre-patterned with 30-nm-deep trenches using electron-beam lithography and $\text{SF}_6\text{-O}_2$ plasma etch. The expected width of epiGNRs is then $\sim 66 \text{ nm}$, determined by the trench depth and the sidewall facet angle (which is 27° from the basal plane). To fabricate FET-like devices, pairs of Pd/Au (20/30 nm thick) contacts were deposited on a selected epiGNR using electron-beam lithography and evaporation. The field effect is provided by an Al top gate with a 41-nm-thick Al_2O_3 gate dielectric. A device schematic and optical microscope image are shown in Fig. 1, and further detailed information about the device fabrication can be found in Ref. 4.

The low-frequency electrical noise of sidewall epiGNRs was measured using an SR780 signal analyzer with a four-terminal

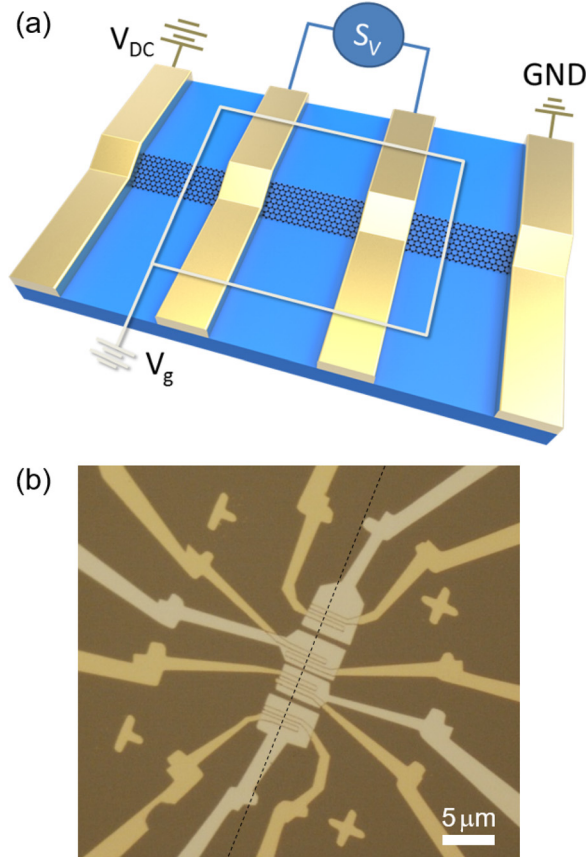


FIG. 1. (a) Artistic representation of the four-terminal measurement configuration of voltage noise across the epiGNR. The top gate (white rectangle) covers the entire junction area (Au/Pd-epiGNR-Pd/Au), while the injection of current into the ribbon uses contacts outside the gated area. The image is not to scale and for illustrative purposes only. (b) Optical microscope image of a device used in this experiment. Gold color indicates the Pd/Au contacts, while light gray color indicates the Al top gates. The epiGNR underneath is marked by the dashed line.

configuration, as portrayed in Fig. 1(a). To eliminate the noise of metal contacts, the DC voltage (V_{DC}) was applied to the epiGNR using a pair of contacts outside the gated area, while the inner contacts were used solely for measuring the bias voltage (V_{bias}) and the noise spectral density (S_V). To minimize the extrinsic noise from measurement electronics, a set of batteries and a voltage divider, both of which were shielded in a metal box, were utilized to provide V_{DC} at a proper level. At zero bias ($V_{bias} = 0$ V), the sidewall epiGNR reveals a low noise level corresponding to the frequency-independent Johnson-Nyquist noise,¹⁷ $S_V = 4k_B TR$, where k_B is the Boltzmann constant, T is the temperature, and R is the resistance of the sample.

When a DC bias is applied across the ribbon, S_V takes on a distinct frequency dependence of $1/f^\gamma$ at low frequencies, with γ close to the expected value of 1 for all twelve samples studied. Figure 2 shows the bias dependence of S_V (sample #1) below 200 Hz measured at 77 K. At low bias, the S_V vs f curve (red line) is just above the estimated Johnson-Nyquist level (dashed line), while at high bias, curves are dominated by the distinct $1/f$ dependence. The measurement at

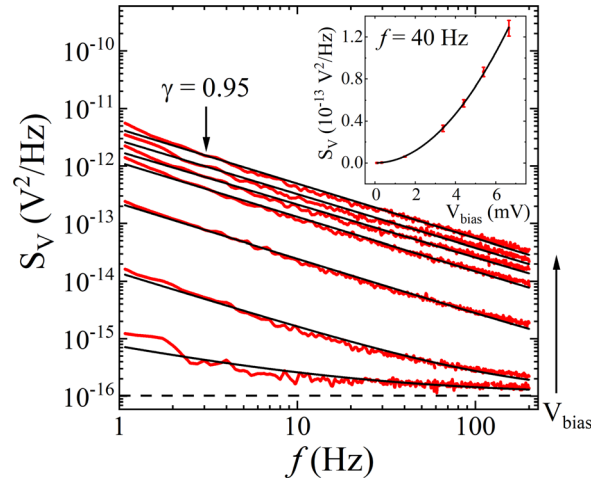


FIG. 2. Bias dependence of the low-frequency noise of sample #1 (red lines) measured at 77 K. The applied bias voltages are $V_{bias} = 0.085, 0.33, 1.48, 3.37, 4.40, 5.39,$ and 6.65 mV, respectively. At low bias, the S_V vs f curve is just above the estimated Johnson-Nyquist level (dashed line, calculated using the measured resistance $R(77\text{ K}) = 23.5$ k Ω). At high bias, curves are dominated by a $1/f^\gamma$ dependence, with the value of γ consistently between 0.9 and 1.1. Black lines are best fits to the data using Eq. (1). Specifically, when $V_{bias} = 6.65$ mV, $\gamma = 0.95$. (Inset) S_V taken at 40 Hz as a function of V_{bias} . The black line is the best fit to the data using Eq. (1) with $f = 40$ Hz and $\gamma = 1$.

the lowest bias also indicates the low noise floor of our experimental setup. Further noise floor reduction would require more advanced cross correlation methods.^{18,19} In this work, we assume incoherence between the Johnson-Nyquist and $1/f$ noise and model S_V as

$$S_V = 4k_B TR + A \frac{V_{bias}^2}{f^\gamma}, \quad (1)$$

with the value of γ consistently between 0.9 and 1.1 for all bias voltages. The dimensionless pre-factor A can be defined as the noise amplitude, a quantity that has been used for comparison across devices.¹⁵ To better determine the value of A , we take a cut of the data in the main panel of Fig. 2 at $f = 40$ Hz and plot the corresponding S_V as a function of V_{bias} in the inset. This allows us to fit $S_V(V_{bias})$ with a simple parabola (black line) for $A = 1.2 \times 10^{-7}$ after setting $\gamma = 1$.

The noise amplitude also depends on the total number of charge carriers (N) or the carrier density (n) in the epiGNR, which can be controlled using the top gate (V_g). Specifically, in the case when the Johnson-Nyquist noise is negligible, Eq. (1) reduces to the Hooge relation,²⁰

$$S_V = \frac{\alpha_H V_{bias}^2}{N f^\gamma}, \quad (2)$$

where the Hooge parameter $\alpha_H = AN$ is a material-dependent constant. To check the $A - N$ or $A - n$ relation in sidewall epiGNR FETs, we take the dielectric constant of Al_2O_3 to be $\epsilon = 7$ and estimate the gate capacitance of our device $C_k = 176$ nF/cm² using an effective model incorporating the fringe-field effect of narrow ribbons.²¹ When we include the contribution of quantum capacitance,²² the resulting equation relating n to the effective gate voltage $V_g^* = V_g - V_{CN}$ reads

$$V_g^* = \frac{e}{C_k} n + \frac{\hbar v_F \sqrt{\pi n}}{e}, \quad (3)$$

where e is the electron charge, \hbar is the reduced Planck's constant, $v_F \approx 1.0 \times 10^6$ m/s is the Fermi velocity, and V_{CN} is the gate voltage corresponding to the charge neutrality point of sidewall epiGNR (typically, $V_{CN} \approx -3$ V in our devices).

Figure 3(a) shows the V_g^* dependence of the resistance R (black line) and noise amplitude A (blue line) of sample #2 measured at room temperature. Sample #2 has a large gate tunable range, suited for V_g^* -dependent studies on both the electron and hole sides. For consistency check, we include the V_g^* -dependence of sample #1 and V_{bias} -dependence of sample #2 in the [supplementary material](#). The results of Fig. 3(a) are then translated to $R(n)$ and $A(n)$ using the $V_g^* - n$ relation of Eq. (3). $A(n)$ (blue line) is plotted in Fig. 3(b) and compared to the normalized resistance derivative $(\frac{dR}{dn})^2/R^2$ (black line) as a function of n . Following Ref. 4, we model the charge transport in sidewall epiGNRs as $G(V_g^*) = G_0 + \frac{ne\mu}{N_{sq}}$, where the conductance

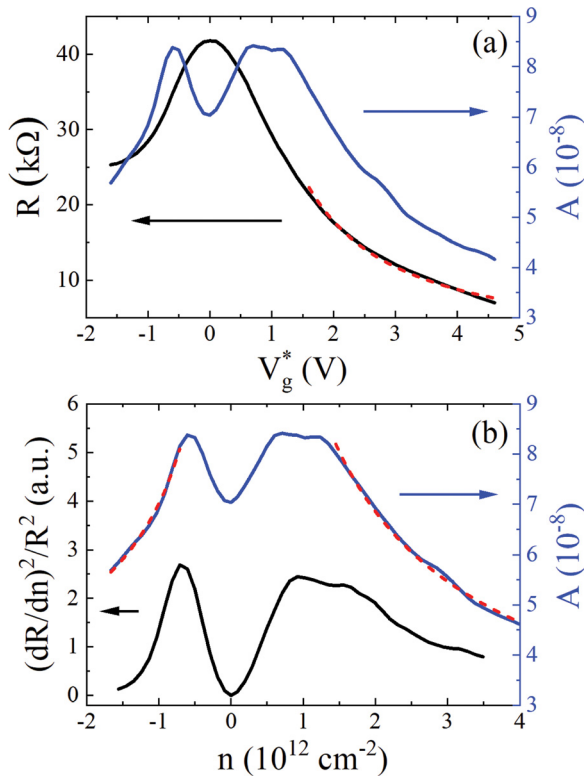


FIG. 3. (a) V_g^* dependence of the resistance R (black) and noise amplitude A (blue) of sample #2 measured at room temperature. The red dashed line is the best fit to $R(V_g^*)$ at high gate voltages using the Drude model. $A(V_g^*)$ shows a characteristic M shape about the charge neutrality point at $V_g^* = 0$ V. (b) Noise amplitude A (blue) and normalized resistance derivative $(\frac{dR}{dn})^2/R^2$ (black) as a function of carrier density n . Red dashed lines are n^β fits for the electron and hole side of the noise amplitude at high carrier densities with $\beta_e = -0.56$ and $\beta_h = -0.42$, respectively.

$G(V_g^*) = 1/R(V_g^*)$, and the first term G_0 describes the contribution from the ballistic edge channel, while the second term describes the diffusive conduction in the bulk using the Drude model. $N_{sq} = 10$ is the total number of squares of the gated epiGNR, and μ is the bulk mobility. We note that although the noise characteristics of the ballistic transport at charge neutrality ($n = 0$) is an interesting topic for future shot noise measurements, in this work, we focus on the low-frequency noise of epiGNRs at high carrier densities, where the transport is well described by the Drude model. The red dashed line in Fig. 3(a) shows the best fit to $R(V_g^*)$ in the high-density regime using $R(V_g^*) = \frac{N_{sq}}{n(V_g^*)e\mu}$. A moderate mobility of $\mu \approx 1700$ $\text{cm}^2 \text{V}^{-1} \text{s}^{-1}$ is obtained, consistent with that reported for gated epitaxial graphene on SiC.¹² The “M” shape of $A(V_g^*)$, however, clearly deviates from the Hooge relation (where $A \propto 1/n$), which is an empirical relation well obeyed by conventional semiconductor FETs²³ and CNT FETs.^{24,25} Such an M shape has been previously reported in graphene FETs,^{26–32} but absent in lithographically patterned exfoliated GNRs.³³ In fact, in Ref. 33, a very weak V_g^* dependence is observed at room temperature. For our sidewall epiGNRs, the decrease in $A(V_g^*)$ at charge neutrality could be due to the presence of dominant ballistic edge transport. At high carrier densities, prior studies of graphene FETs on Si/SiO₂ substrates attribute the decreasing A to charge traps (shallowly) embedded in SiO₂ near the graphene/SiO₂ interface.^{32,33} In our epiGNR FETs, similar charge traps may exist in Al₂O₃.

To better understand the $A - n$ relation in sidewall epiGNRs, we follow the model of Ref. 30 and consider the n - and μ -fluctuations as the main mechanisms of $1/f$ noise at high carrier densities. Specifically, since μ is a function of n and n_{imp} , we can break down the resistance fluctuation as follows:

$$\delta R = \frac{dR}{dn} \delta n + \frac{dR}{dn_{imp}} \delta n_{imp}, \quad (4)$$

where the first term leads to $A \propto (\frac{\delta R}{R})^2 \propto (\frac{dR}{dn})^2/R^2$, and the second term depends on the scattering mechanisms in our devices. Indeed, as one can see from Fig. 3(b): (i) the normalized resistance derivative $(\frac{dR}{dn})^2/R^2$ (black line) exhibits a similar M shape to $A(n)$ (blue line) and (ii) clear differences between $(\frac{dR}{dn})^2/R^2$ and $A(n)$ appear at charge neutrality and high carrier densities where $(\frac{dR}{dn})^2/R^2 \rightarrow 0$ but A remains finite. At a sufficiently high density, A is expected to be dominated by the second term in Eq. (4), providing important information on the dominant scattering mechanism. Therefore, we perform n^β fits to experimental data $A(n)$ at high densities. Given that $R(n) = \frac{N_{sq}}{ne\mu}$ in our sidewall epiGNRs [red dashed line in Fig. 3(a)], when the main source of fluctuations is short-range scatters,³⁴ δR_{sr} is independent of n and $A(n) \propto [\frac{1}{R(n)}]^2 \propto n^2$ (i.e., $\beta = 2$). On the other hand, when the main source of fluctuations is long-range scatters,³⁵ $\delta R_{lr} \propto 1/n$ and $A(n)$ is independent of n (i.e., $\beta = 0$). The red dashed lines in Fig. 3(b) show the best n^β fits to $A(n)$ with $\beta_e = -0.56$ and $\beta_h = -0.42$, respectively. The fitting results indicate that long-range scatters are the main source of $1/f$ noise at high carrier densities, while

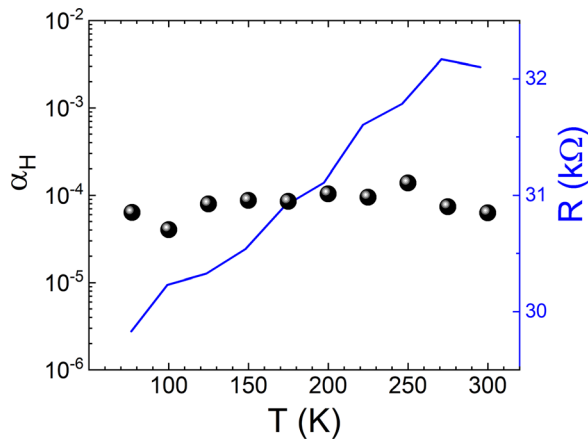


FIG. 4. Temperature dependence of the Hooge parameter α_H (spheres) and resistance R (line) of sample #3 measured between 300 and 77 K. α_H remains approximately constant at 8.3×10^{-5} throughout the temperature range, while R decreases modestly at lower temperatures. α_H was taken at $V_g^* = 0.95$ V at each temperature (constant n), corresponding to a peak in A in Fig. 3(a).

the derivation from $\beta = 0$ can be simply due to the contribution of non-vanishing $\left(\frac{dR}{dn}\right)^2/R^2 \propto n^{-2}$ from the first term of Eq. (4). Similar β values were also reported in Ref. 30 and attributed to long-range scatters (charge traps) in Si/SiO₂ substrates.

Next, we examine the temperature dependence of $1/f$ noise in our sidewall epiGNRs. In Fig. 4, we plot the measured Hooge parameter α_H (spheres) of sample #3 between room temperature (300 K) and liquid nitrogen temperature (77 K). Different from samples #1 and #2, sample #3 was grown on the sidewall of a 40-nm-deep trench, resulting in a larger surface area. α_H was taken at $V_g^* = 0.95$ V at each temperature (with constant n and, thus, $\alpha_H \propto A$), corresponding to a peak in A in Fig. 3(a). The selected V_g^* is also close to a peak in $\left(\frac{dR}{dn}\right)^2/R^2$, where R is most sensitive to density fluctuations. Experimentally, we find that α_H remains approximately constant at 8.3×10^{-5} throughout the temperature range, while R decreases modestly at lower temperatures. The lack of temperature dependence in A is in sharp contrast to the prior studies of lithographically patterned exfoliated GNRs,³³ where A is significantly enhanced at 77 K due to edge disorder and the resulting hopping-dominated charge transport. In our sidewall epiGNRs, the crystallinity of the edges is well preserved by connecting either to the SiC substrate (bottom edge) or to the buffer layer (top edge) on the top surface.^{4,36} We further note that since the long-range scatters (charge traps) at the epiGNR/gate-dielectric interface are the dominant noise source at high carrier densities, we expect two competing temperature dependencies in the noise amplitude. On the one hand, when we lower the temperature, some active charge traps may freeze, leading to noise reduction. On the other hand, since $R(n) = \frac{N_{sq}}{ne\mu}$ and $\delta R_{lr} \propto 1/n$, the second term in Eq. (4) gives rise to $A(n) \propto \left(\frac{\delta R_{lr}}{R}\right)^2 \propto \mu^2$, which increases with decreasing temperature.³⁷ The competition of these two effects results in the observed temperature dependence.

Finally, we comment on the low noise amplitude of sidewall epiGNR FETs. The Hooge parameter α_H has been widely used as the

figure of merit for $1/f$ noise to compare among electronic systems. In our sidewall epiGNR FETs, $\alpha_H < 10^{-4}$ at room temperature, one order of magnitude better than $\alpha_H \sim 10^{-3}$ of the conventional semiconductor and CNT FETs.^{24,25} When compared with previous graphene-based devices, our results are in line with high-quality suspended graphene^{28,29} and graphene on hexagonal boron nitride substrates,^{31,32,38} which is more than one order of magnitude lower than that in exfoliated graphene on Si/SiO₂ substrates and 5–10 times lower than lithographically patterned GNRs.^{39,40} Also, we find that the dominant noise source in our devices is extrinsic, due to the long-range scatters at the epiGNR/gate-dielectric interface, therefore holding promise for further improvements. Previous studies of $1/f$ noise in the bilayer and few-layer graphene have shown a strong reduction in noise.^{39,41–43} Fabricating multilayer epiGNR FETs is, thus, an alternative possibility.

In summary, we perform low-frequency noise measurements on gated sidewall epiGNRs and reveal a low level of $1/f$ noise at room temperature. At low temperatures, in contrast to prior studies of lithographically patterned exfoliated GNRs, our sidewall epiGNR FETs do not show a visible increase in noise amplitude, indicating that the charge transport is not in the hopping regime and edge disorder is not a serious concern. Further quantitative analysis of the gate dependent noise amplitude suggests that long-range scatters (presumably at the epiGNR/gate-dielectric interface) are likely to be the main source of the noise at high carrier densities, which can in principle be reduced via improving the fabrication method or increasing the number of graphene layers. Our results support the potential use of sidewall epiGNRs for high signal-to-noise ratio device applications such as interconnects, chemical sensors, and radiation detectors.

See the [supplementary material](#) for additional experimental data.

We thank Jeremy Yang for assistance in epiGNR device fabrication. This work was supported by the NSF (Grant Nos. DMR-0820382, DMR-1308835, and ECCS-1506006) and the NASA Solar System Exploration Research Virtual Institute (Cooperative Agreement No. NNA17BF68A). O.V. acknowledges the NSF EAPSI program (Grant No. OISE-1614176), and C.B. acknowledges partial funding from the EU flagship graphene (Grant Nos. 696656 and 785219) and French National Research Agency (Grant No. AAP CE24 BONNEG). C.B. and Z.J. also acknowledge the Thomas Jefferson grant from the French-American Cultural Exchange Council. The epiGNR device fabrication was performed in part at the Georgia Tech Institute for Electronics and Nanotechnology, a member of the National Nanotechnology Coordinated Infrastructure, which is supported by the NSF (Grant No. ECCS-1542174).

DATA AVAILABILITY

The data that support the findings of this study are available from the corresponding author upon reasonable request.

REFERENCES

- S. V. Morozov, K. S. Novoselov, M. I. Katsnelson, F. Schedin, D. C. Elias, J. A. Jaszczak, and A. K. Geim, *Phys. Rev. Lett.* **100**(1), 016602 (2008).
- J.-H. Chen, C. Jang, S. Xiao, M. Ishigami, and M. S. Fuhrer, *Nat. Nanotechnol.* **3**(4), 206–209 (2008).

- ³L. Wang, I. Meric, P. Y. Huang, Q. Gao, Y. Gao, H. Tran, T. Taniguchi, K. Watanabe, L. M. Campos, D. A. Muller, J. Guo, P. Kim, J. Hone, K. L. Shepard, and C. R. Dean, *Science* **342**(6158), 614–617 (2013).
- ⁴J. Baringhaus, M. Ruan, F. Edler, A. Tejada, M. Sicot, A. Taleb-Ibrahimi, A. P. Li, Z. Jiang, E. H. Conrad, C. Berger, C. Tegenkamp, and W. A. de Heer, *Nature* **506**(7488), 349–354 (2014).
- ⁵M. Y. Han, B. Özyilmaz, Y. Zhang, and P. Kim, *Phys. Rev. Lett.* **98**(20), 206805 (2007).
- ⁶Z. Chen, Y.-M. Lin, M. J. Rooks, and P. Avouris, *Physica E* **40**(2), 228–232 (2007).
- ⁷D. V. Kosynkin, A. L. Higginbotham, A. Sinitskii, J. R. Lomeda, A. Dimiev, B. K. Price, and J. M. Tour, *Nature* **458**(7240), 872–876 (2009).
- ⁸L. Jiao, L. Zhang, X. Wang, G. Diankov, and H. Dai, *Nature* **458**(7240), 877–880 (2009).
- ⁹W. A. de Heer, *MRS Bull.* **29**(04), 281–285 (2004).
- ¹⁰M. Y. Han, J. C. Brant, and P. Kim, *Phys. Rev. Lett.* **104**(5), 056801 (2010).
- ¹¹W. A. de Heer, C. Berger, M. Ruan, M. Sprinkle, X. Li, Y. Hu, B. Zhang, J. Hankinson, and E. Conrad, *Proc. Natl. Acad. Sci.* **108**(41), 16900–16905 (2011).
- ¹²C. Berger, E. Conrad, and W. A. de Heer, in *Landolt-Börnstein: Numerical Data and Functional Relationships in Science and Technology-New Series, Vol. 45, Physics of Solid Surfaces, Subvolume B-VIII*, edited by G. Chiarotti and P. Chiaradia (Springer-Verlag Berlin Heidelberg, 2018), pp. 665–748.
- ¹³M. Sprinkle, M. Ruan, Y. Hu, J. Hankinson, M. Rubio-Roy, B. Zhang, X. Wu, C. Berger, and W. A. de Heer, *Nat. Nanotechnol.* **5**(10), 727–731 (2010).
- ¹⁴A. De Cecco, V. S. Prudkovskiy, D. Wander, R. Ganguly, C. Berger, W. A. de Heer, H. Courtois, and C. B. Winkelmann, *Nano Lett.* **20**(5), 3786–3790 (2020).
- ¹⁵A. A. Balandin, *Nat. Nanotechnol.* **8**(8), 549–555 (2013).
- ¹⁶C. Berger, D. Deniz, J. Gigliotti, J. Palmer, J. Hankinson, Y. Hu, J.-P. Turmaud, R. Puybaret, A. Ougazzaden, A. N. Sidorov, Z. Jiang, and W. A. de Heer, in *Growing Graphene on Semiconductors*, edited by N. Motta, F. Iacopi, and C. Coletti (Psychology Press, 2017).
- ¹⁷H. Nyquist, *Phys. Rev.* **32**(1), 110–113 (1928).
- ¹⁸M. Marzano, A. Cultrera, M. Ortolano, and L. Callegaro, *Meas. Sci. Technol.* **30**(3), 035102 (2019).
- ¹⁹A. Cultrera, L. Callegaro, M. Marzano, M. Ortolano, and G. Amato, *Appl. Phys. Lett.* **112**(9), 093504 (2018).
- ²⁰F. N. Hooge, *Phys. Lett. A* **29**(3), 139–140 (1969).
- ²¹H. B. Palmer, *Trans. Am. Inst. Electr. Eng.* **56**(3), 363–366 (1937).
- ²²T. Fang, A. Konar, H. Xing, and D. Jena, *Appl. Phys. Lett.* **91**(9), 092109 (2007).
- ²³A. L. McWhorter and R. H. Kingston, *Semiconductor Surface Physics* (University of Pennsylvania Press, 1957).
- ²⁴P. G. Collins, M. S. Fuhrer, and A. Zettl, *Appl. Phys. Lett.* **76**(7), 894 (2000).
- ²⁵D. Tobias, M. Ishigami, A. Tselev, P. Barbara, E. D. Williams, C. J. Lobb, and M. S. Fuhrer, *Phys. Rev. B* **77**(3), 033407 (2008).
- ²⁶I. Heller, S. Chatoor, J. Männik, M. A. G. Zevenbergen, J. B. Oostinga, A. F. Morpurgo, C. Dekker, and S. G. Lemay, *Nano Lett.* **10**(5), 1563–1567 (2010).
- ²⁷G. Xu, C. M. Torres, Jr., Y. Zhang, F. Liu, E. B. Song, M. Wang, Y. Zhou, C. Zeng, and K. L. Wang, *Nano Lett.* **10**(9), 3312–3317 (2010).
- ²⁸A. N. Pal, S. Ghatak, V. Kochat, E. S. Sneha, A. Sampathkumar, S. Raghavan, and A. Ghosh, *ACS Nano* **5**(3), 2075–2081 (2011).
- ²⁹Y. Zhang, E. E. Mendez, and X. Du, *ACS Nano* **5**(10), 8124–8130 (2011).
- ³⁰A. A. Kaverzin, A. S. Mayorov, A. Shytov, and D. W. Horsell, *Phys. Rev. B* **85**(7), 075435 (2012).
- ³¹M. A. Stolyarov, G. Liu, S. L. Rumyantsev, M. Shur, and A. A. Balandin, *Appl. Phys. Lett.* **107**(2), 023106 (2015).
- ³²M. Kayyalha and Y. P. Chen, *Appl. Phys. Lett.* **107**(11), 113101 (2015).
- ³³G. Xu, C. M. Torres, E. B. Song, J. Tang, J. Bai, X. Duan, Y. Zhang, and K. L. Wang, *Nano Lett.* **10**(11), 4590–4594 (2010).
- ³⁴N. H. Shon and T. Ando, *J. Phys. Soc. Jpn.* **67**(7), 2421–2429 (1998).
- ³⁵T. Ando, *J. Phys. Soc. Jpn.* **75**(7), 074716 (2006).
- ³⁶W. Norimatsu and M. Kusunoki, *Physica E* **42**(4), 691–694 (2010).
- ³⁷A. N. Pal, A. A. Bol, and A. Ghosh, *Appl. Phys. Lett.* **97**(13), 133504 (2010).
- ³⁸X. Li, X. Lu, T. Li, W. Yang, J. Fang, G. Zhang, and Y. Wu, *ACS Nano* **9**(11), 11382–11388 (2015).
- ³⁹Y.-M. Lin and P. Avouris, *Nano Lett.* **8**(8), 2119–2125 (2008).
- ⁴⁰G. Xu, J. Bai, C. M. Torres, E. B. Song, J. Tang, Y. Zhou, X. Duan, Y. Zhang, and K. L. Wang, *Appl. Phys. Lett.* **97**(7), 073107 (2010).
- ⁴¹A. N. Pal and A. Ghosh, *Phys. Rev. Lett.* **102**(12), 126805 (2009).
- ⁴²A. N. Pal and A. Ghosh, *Appl. Phys. Lett.* **95**(8), 082105 (2009).
- ⁴³Q. Shao, G. Liu, D. Teweldebrhan, A. A. Balandin, S. Rumyantsev, M. S. Shur, and D. Yan, *IEEE Electron Device Lett.* **30**(3), 288–290 (2009).